The intriguing role of collagen on the rheology of cancer cell spheroids

Daria Tsvirkun, Jean Revilloud, Arianna Giannetti, Claude Verdier

The intriguing role of collagen on the rheology of cancer cell spheroids

Daria Tsvirkun[a], Jean Revilloud[a], Arianna Giannetti[a], Claude Verdier[1 a]

[a] *Université Grenoble Alpes, CNRS, LIPhy, Grenoble, 38000, France*

Abstract

Spheroids are multicellular systems with an interesting rheology giving rise to elasto–visco–plastic properties. They are good tumor models, but the role of the extra–cellular matrix (ECM) is not fully understood. Yet ECM is an important link between cells and may have significant effects. Here we determine viscoelastic properties of spheroids including different collagen amounts using AFM and predict new frequency–dependent properties leading to soft glassy rheology behavior. A unified model – similar to single cell behavior – is proposed and discussed, while complementary confocal experiments reveal the fine microstructure of spheroids, with collagen fibers serving as a skeleton for cells, thus reinforcing the spheroid viscoelastic behavior.

Keywords: cancer cells, viscoelastic, confocal microscopy, AFM

PACS: 87.15.La, 87.18.Ed, 87.19.xj

2000 MSC: 74L15, 92C10, 74D05

1. Introduction

While the mechanical properties of cancer cells have been extensively studied in the litterature (Lekka et al. (1999); Cross et al. (2007); Abidine et al. (2015); Yubero et al. (2020)), the tissue

[1] claude.verdier@univ-grenoble-alpes.fr

scale remains less explored; therefore it is important to understand how cellular properties combine together and whether the local rheology is retained or changed at a higher scale.

Tissues are usually made of cells surrounded by the extra–cellular matrix (ECM) inside a fluid (Fung (1993)), so that concentrations of the different components are important to characterize the full tissue. In particular the amount of fluid may give rise to strong rate–dependent properties. As for the ECM behaving usually as a physical gel, its rheology is well represented by a viscoelastic behavior. Concentrated cell suspensions have been considered using mixture models and exhibit a behavior close to that of yield stress fluids, when the cell volume concentration is around 50% or more (Iordan et al. (2008); Preziosi et al. (2010)). On the other end, with a large collagen content and a small amount of cells included (around 10%), the behavior becomes viscoelastic (Iordan et al. (2010)), and the effect of cells on the ECM is essential, since they are able to remodel the collagen network. Here we pay interest to tissue models containing a large amount of cells with small amounts of ECM within a fluid medium (i.e. culture medium). To investigate such biological tissues, in particular solid tumors, multicellular spheroids have been developed over the years (Netti et al. (1996); Delarue et al. (2013); Weiswald et al. (2015)) and are considered to be outstanding *in vitro* models in cancer research. They are made of an initial number of cells grown in culture medium until cells become closely packed together. Cells within spheroids can also produce their own ECM, as well as they express cell adhesion molecules (e.g. cadherins) to bind together.

With regard to *in vivo* tumors, the amount of ECM or collagen is not so well quantified but it is known that the microenvironment affects cancer cell motility a lot, and can serve as a guide, especially when cells contract to align collagen fibers (Levental et al. (2007); Mierke (2019)).

Furthermore the interactions between collagen–rich tissues at the tumor–stromal boundary can be an important cause of tumorigenesis and invasion (Provenzano et al. (2006); Kai et al. (2019)), since collagen structures polymerize around cells or tumors and form bundles or wavy structures (Natarajan et al. (2019)). Furthermore, it was shown that there is a negative correlation between patient survival and collagen content (Whatcott et al. (2015)). This is why collagen can be considered as a potential tool for tumor therapy due its strong interactions with cancer cells (Quarto et al. (2014); Xu et al. (2019)).

Several earlier studies have focused on the role of compressive stresses (mechanical or osmotic origin) exerted by the outside onto the tumor (Helmlinger et al. (1997)) or spheroid (Delarue et al. (2014)), leading to limited growth. Fewer results are devoted to the understanding of the mechanical behavior of such spheroids (as in Marmottant et al. (2009)), but some models focused on the flow of the interstitial liquid within the spheroids (Netti et al. (1996); Delarue et al. (2013)) revealing that poroelastic active models can fully describe them (Dolega et al. (2021)). Time is therefore an essential parameter, that is why it is important to study frequency–dependent properties, i.e. viscoelastic ones. Such effects have already been observed on tissues like cartilage or tendons, revealing notable high-frequency poroelastic responses (Nia et al. (2013); Connizzo and Grodzinsky (2017)), which can be used to differentiate physiological and pathological tissues. Although these systems are different, possible comparisons can be proposed.

In this work, AFM was chosen as an interesting approach to probe spheroids, made of bladder cancer cells already investigated (Abidine et al. (2015, 2018)). Spheroids preparation is described in Section 2.1, as well as the microrheology technique developed earlier (Giannetti et al. (2020); Abidine et al. (2021)) to probe the spheroids viscoelastic properties (Section 2.2). A simplified

rheological model is used to extract relevant parameters (Section 2.3). Complementary confocal microscopy experiments are described in Section 2.4. This leads to the results presented in Section 3 where the effect of collagen (i.e. the ECM) is emphasized as a proxy linking cells, therefore enhancing the viscoelastic properties. This effect is further discussed in Section 4.

2. Methods

2.1. Multicellular spheroids preparation

In this study we used T24 epithelial bladder cancer cells of invasive type (ATCC, HTB–4, Manassas, VA). These cells are poorly differentiated and very malignant. The choice of such bladder cell lines is guided by previous works (Chotard-Ghodsnia et al. (2007); Haddad et al. (2010); Laurent et al. (2014); Rajan et al. (2017)). T24 cells were cultured in RPMI 1640 (Gibco, Saint-Aubin, France) supplemented with 10% (v/v) fetal bovine serum (FBS, Life Technologies SAS, Villebon-sur-Yvette, France) and 1% (v/v) penicillin-streptomycin solution (Life Technologies SAS). Cells have been stably transfected with a plasmid expressing LifeAct–GFP to stain F–actin (Riedl et al. (2008)). Cells were stored at 37°C in a humidified atmosphere and 5% CO_2.

Previously (Giannetti et al. (2020)), we used 96-well plates covered by 1.5% ultra–pure agarose to culture such spheroids but possible adhesion to the bottom still occurred. Here we chose another method based on spheroid production in hanging drops. First the cover part of the Petri dishes were coated with a PDMS layer (w/w mixture of Stilgar PDMS 9/10 and crosslinker 1/10, baked at 60°C for 2 hours). PDMS is a non toxic and biocompatible material with hydrophobic properties which can hold microscale drops without cellular adhesion even in the presence of extracellular matrix molecules (Kuo et al. (2017)). To form hanging drops, a T24 cell suspension was prepared and

mixed with collagen I rat tail (Corning, Bedford, MA, USA) within culture medium, at different concentrations (c_0) of 0, 0.01 and 0.03 mg/mL at 4 °C and pH ~ 7.4). Cellular drops of 15 μL and 5,000 cells each were dispensed on the PDMS surface (see Figure 1). The cover part with drops was flipped onto the lower part of the Petri dish filled with DPBS to avoid evaporation and drying of drops, and kept for three days at 37°C in a humidified atmosphere and 5% CO_2.

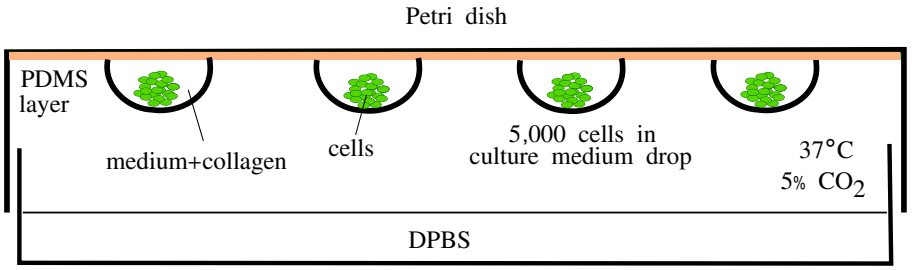

Figure 1: Preparation of spheroids: 15 μL drops containing 5,000 cells (green) in culture medium with (or without) collagen are laid in the Petri dish cover (pretreated with a PDMS layer) which is eventually flipped onto the lower part, so that spheroids can form and do not adhere to the top of the Petri dish.

Cells remained at the bottom of the droplet and aggregated in time. After 3 days, spheroids usually presented a spherical, compact shape (typical spheroid diameter D between 200 and 350 μm, see Figure 2). Spheroids in medium were then caught using a chopped cone (200 μL) and deposited into a TPP Petri dish (used for AFM). After sedimentation and low adhesion to the bottom, culture medium was poured (2 mL) gently around the spheroid. The pre–calibrated AFM cantilever was then lowered to come into contact with the spheroid (Figure 3a). Measurements were carried out as explained below (Section 2.2).

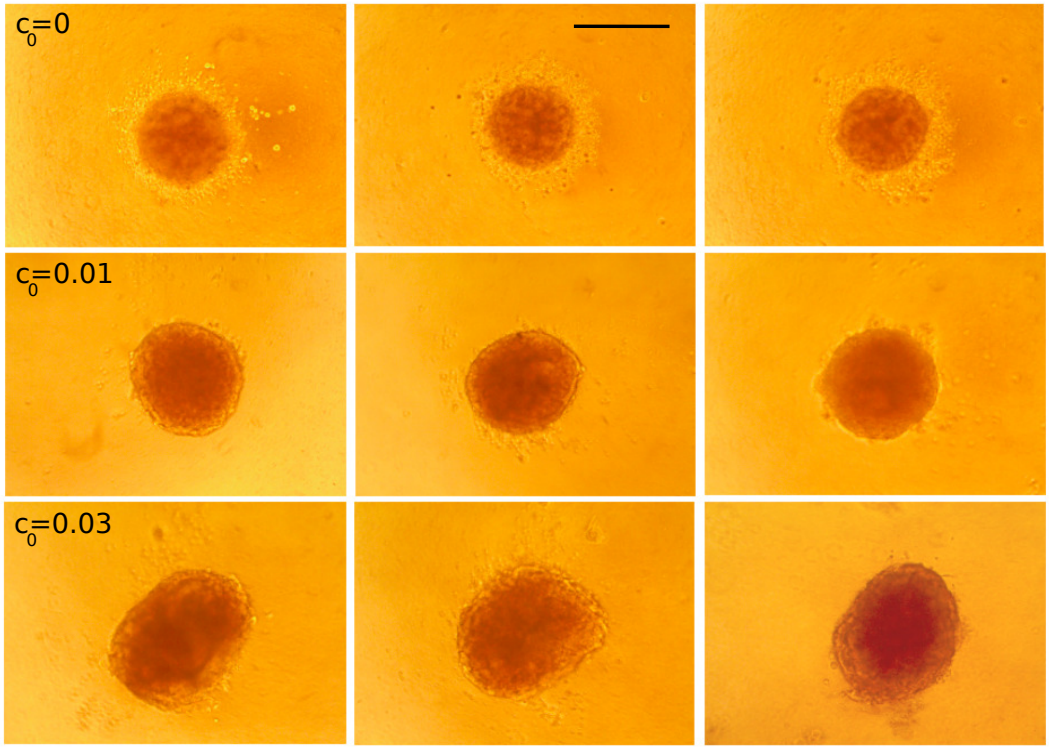

Figure 2: Role of collagen concentration c_0 on spheroid size and microstructure. Three preparations are shown on each line for different collagen concentrations. Top row: c_0 = 0 mg/mL, middle row: c_0 = 0.01 mg/mL, bottom row: c_0 = 0.03 mg/mL. Scale bar = 200 μm (same for all images).

2.2. AFM in force modulation

AFM experiments were achieved using a Nanowizard II AFM (JPK Instruments, Berlin) mounted on a Zeiss microscope (Observer D1), in liquid environment (i.e. culture medium) at 37°C. The AFM technique is based on the use of a tip placed on a cantilever that can be set in contact with a surface to investigate the forces due to the interactions between the tip and the substrate. The laser reflected by the cantilever onto a photodiode gives the tip displacement and therefore the force thanks to proper calibration. Calibration was performed here for the sensibility parameter ($s \sim$ 30–50 nm/V), then using the thermal fluctuation method (Butt and Jaschke (1995)) to finally

obtain the cantilever stiffness (typically k $\sim$ 30 N/m). The basic idea is to perform an initial indentation δ_0, then to superimpose small sinusoidal deformations δ at a given frequency f. This is shown in Figure 3b, where the initial approach is followed by oscillation of the piezo at frequencies increasing from 1 to 32 Hz in this case. Note that linear theory is verified since both piezo height Z(t) and force F(t) oscillate at the same frequency. For spheroids, we use large tipless cantilevers (Nanosensors, TL-NCL model, 225μm in length, and 38 μm in width, see Giannetti et al. (2020)) indenting the spheroid. This flat cantilever applies initial indentations on the order $\delta_0 \sim$ 4–8 μm, corresponding to contact radii $\sim$ 20–40 μm, and an area of contact $\sim$ 1200–5000 μm^2. As cells are connected to each other, indentation involves the whole spheroid response. The Hertz formula relates the applied force F_0 to the indentation δ_0. Here the rigid flat cantilever is in contact with the soft spheroid, so the relationship between F_0 and δ_0 reads: $F_0 = \frac{4}{3}\frac{E\sqrt{R}\delta_0^{3/2}}{1-\nu^2}$ where E is the Young's spheroid modulus, ν its Poisson ratio ($\nu \sim 0.5$) and R is the radius of the spheroid. After linearization, i.e. F_0 is replaced by $F_0 + F$, and δ_0 becomes $\delta_0 + \delta$, with the only first order terms retained, one finds (Cai et al. (2013)):

$$G^*(\omega) = G' + i\,G" = \frac{1-\nu}{4\sqrt{R\delta_0}}\left\{\frac{F^*(\omega)}{\delta^*(\omega)} - i\,\omega b(0)\right\} \tag{1}$$

where ω is the angular frequency in rad/s, and $\omega = 2\pi f$, f being the frequency (Hz). In Equation (1), the hydrodynamic drag has been calibrated by oscillating the cantilever in the fluid: the drag is proportional to viscosity and velocity, but also depends on geometry. Starting far from the substrate at a distance h, and getting closer (decreasing h), we determine the purely viscous drag force in the form $F^*/\delta^* = i\omega b(h)$. $b(h)$ is obtained experimentally and extrapolated as h $\to$ 0,

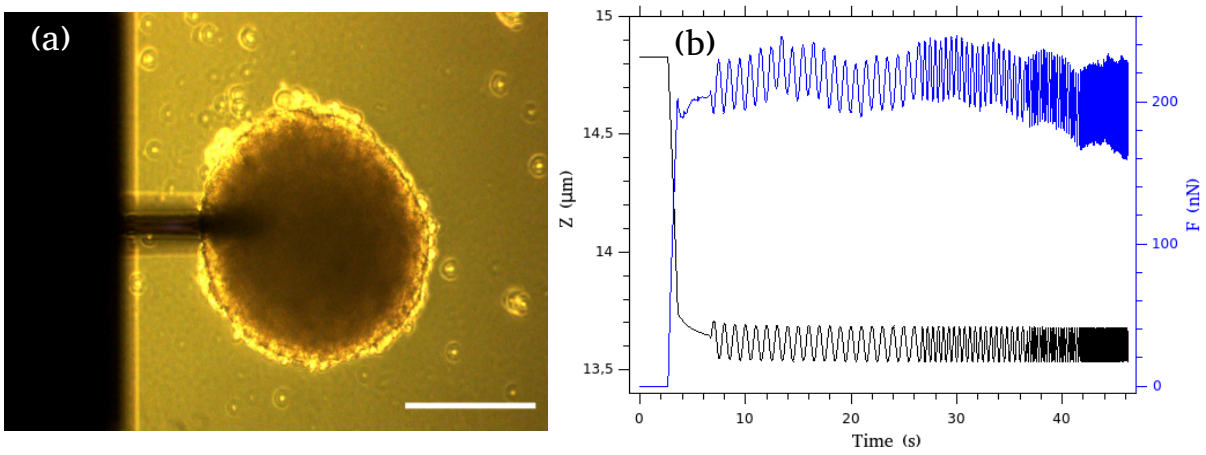

Figure 3: (a) Microscopy image of the AFM cantilever close to the top of the spheroid (c_0 = 0 mg/mL, R ~ 175 μm). Scale bar = 200 μm. (b) Typical applied piezo height $Z(t)$ (black) and measured $F(t)$ (blue), corresponding to the approach of the cantilever for an applied force F_0 = 200nN, relaxation for 4 s, followed by oscillations at 1 Hz, 2 Hz, 4 Hz, 8 Hz, 16 Hz, 32 Hz. Piezo height $Z(t)$ and force $F(t)$ vary at the same frequency, but signals exhibit a phase shift.

providing the value of $b(0)$ as explained by Alcaraz et al. (2002). Here we found b(0) = 3.45 10^{-5} N.s/m. Therefore, using this method, it is possible to obtain the viscoelastic data (G',G") over a large range of frequency, typically from 1 Hz to 1 kHz.

2.3. Rheological model

Different authors have tried to model viscoelastic data, in particular studying polymers or complex materials (Palade et al. (1996); Sollich et al. (1997); Fabry et al. (2001)) with a wide relaxation time spectra showing power law dependence, i.e., moduli G' and G'' vary with a power of the frequency f. For example, it was reported that cells have moduli (G', G'') varying with a small exponent ~ 0.1–0.3 at low frequencies (Trepat et al. (2008); Alcaraz et al. (2003)), and could

behave as Newtonian fluids (with viscosity η) at larger frequencies, therefore exhibiting moduli of the form $G^*(\omega) = G\,(i\omega\tau)^\alpha + i\omega\eta$ (Alcaraz et al. (2003)), where τ is a typical time scale, and G is an elastic modulus. Usually a single exponent is not enough to cover the whole frequency range; therefore, it is better to define several frequency domains with different exponents (Stamenovic et al. (2007); Abidine et al. (2015, 2018)). Our data suggests that G' varies with one exponent only (slope a) whereas two exponents (b and c) are necessary to describe G'' depending on the frequency range. For this reason, the following model is proposed:

$$G' = G_0\,(\frac{f}{f_0})^a\,, \qquad G'' = G_1\,(\frac{f}{f_0})^b + G_2\,(\frac{f}{f_0})^c \tag{2}$$

Note that we can use $f_0 = 1$ Hz, therefore f is expressed in Hz, for simplicity. By making this dimensionless reduction, we can get rid of the complex prefactor units. Indeed, G_0, G_1, G_2 are expressed in Pascals (Pa), whereas exponents a, b, c are dimensionless. The next comparison concerns previous data found for single cells (Fabry et al. (2001); Alcaraz et al. (2003); Abidine et al. (2021)) where it was shown that in some cases $a = b$ and $c = 1$.

2.4. Confocal microscopy

Confocal imaging of spheroids containing 0, 0.01 or 0.03 mg/mL collagen was carried out using a confocal Leica TCS SP8 (LIPhy platform). Cells with F-actin GFP labeling were imaged in the green channel (argon laser, 488 nm), and collagen was imaged using the reflectance technique in the red channel (HeNe laser, 633 nm) following previous works (Friedl et al. (2001); Abidine et al. (2021)). The spheroids were prepared as described earlier and allowed to settle in a Petri dish (with a 170 μm glass coverslip glued at the bottom). Petri dishes were set on the pre-heated micro-

scope (37°C). Spheroids (usually 200-250 μm in size) were imaged using a Leica APO 40×/1.30 Oil objective and Zoom ×0.75, starting from the bottom to the top. Z-stacks were acquired using steps of 0.35 μm. For each image given, we used 5 slices located around the mid–plane and made a Z–projection to enhance the intensity, and reduce noise.

2.5. Statistics

Statistical analysis to compare the three cases was done using one–way ANOVA. At least $N > 10$ spheroids were measured. Statistical significance was reached for $*p < 0.05$, $**p < 0.01$, $***p < 0.001$, while $p > 0.05$ was considered non significant. Means are presented together with the standard error of the mean (SEM).

3. Results

3.1. Rheology and modelling

Spheroids prepared in the collagen extra-cellular matrix were studied using three collagen concentrations c_0 of 0 mg/mL, 0.01 mg/mL and 0.03 mg/mL. This concentration is low enough in order to avoid collagen polymerisation at 37°C. The dynamic moduli G' and G" were measured in the [1–1000Hz] frequency range by using frequencies that are multiples of 2 (1Hz, 2Hz, 4Hz ... until 1024 Hz), so that a logarithm variation is obtained (around 3 points per decade). Results are shown below in Figure 4.

Note that points at low frequencies, typically around 1 Hz, can give rise to active reaction of the cells within the spheroids, therefore noise was found. Altogether the data was averaged (N>10) and showed some intriguing effects due to the presence of the collagen extra-cellular matrix. The

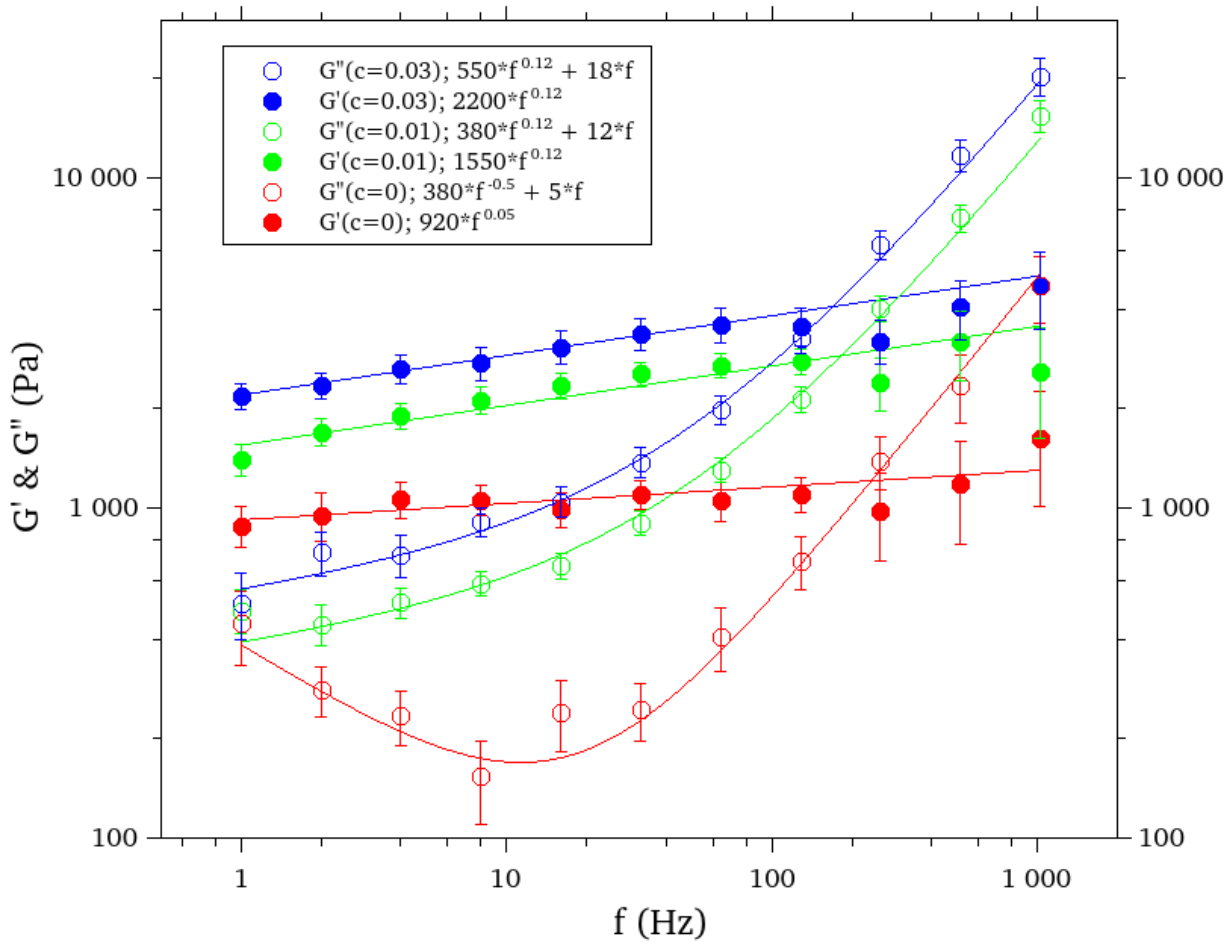

Figure 4: Viscoelastic moduli G' (filled circles) and G"(empty circles) for collagen concentrations c_0 = 0 (red, N=14), c_0 = 0.01 mg/mL (green, N=11), and c_0 = 0.03 mg/mL (blue, N=11). Fits obtained with the model are also provided in the legend. Error bars indicate mean value +/- SEM.

model presented in the previous Section 2.3 was used to predict the different behaviors observed. For all frequencies, power laws were found regarding the elastic component G'. On the other hand, the loss modulus G" exhibited a typically power law at low frequencies (the same as G' in the case of spheroids including collagen), and a slope of 1 at higher frequencies typical of a viscous behavior, as already observed for cells (Alcaraz et al. (2003); Abidine et al. (2021)).

c_0(mg/mL)	G_0(Pa)	G_1(Pa)	G_2(Pa)	a	b	c	$f_T(Hz)$
0	920	380	5	0.05	-0.5	1	197
0.01	1550	380	12	0.12	0.12	1	182
0.03	2200	550	18	0.12	0.12	1	170

Table 1: Parameters are defined by: $G' = G_0\, f^a$ and $G'' = G_1\, f^b + G_2\, f^c$, using f_0=1Hz, and f is expressed in Hz. f_T is the transition frequency corresponding to the crossing $G' = G''$. Fitting was obtained using the mean values of G' and G" at each frequency.

Using these observations, fitting of the moduli G' and G" gave the following results $G' = G_0\, f^a$ and $G'' = G_1\, f^b + G_2\, f^c$, indicated in the legend of Figure 4 after using f_0=1Hz (thus f is in Hz for simplicity). These parameters are listed in Table 1 below.

Further comparisons of the viscoelastic data can be made through simple statistics of the changes in moduli G' and G''. For example, in Figure 5, we selected a typical frequency, 8Hz, lying in the mid–range and compared moduli for different collagen concentrations. Moduli G'(8Hz) are significantly different between spheroids at different concentrations (significance p from one–way ANOVA test: 0–0.01mg/mL, p=8.13 10^{-5}, 0–0.03mg/mL, p=1.80 10^{-6}, 0.01–0.03mg/mL, p=0.0343), and similarly for G''(8Hz) (significance p: 0–0.01mg/mL, p=7.57 10^{-8}, 0–0.03mg/mL, p=1.36 10^{-8}, 0.01–0.03mg/mL, p=0.0106). There is obviously an effect of the collagen on multicellular spheroids, which is shown by this rheology data. To summarize:

- At $c_0 = 0$, the spheroid behaves as an elastic material with an almost constant plateau modulus $G_0 \sim 1000$ Pa (or a very small power law exponent a=0.05), and a loss modulus decreas-

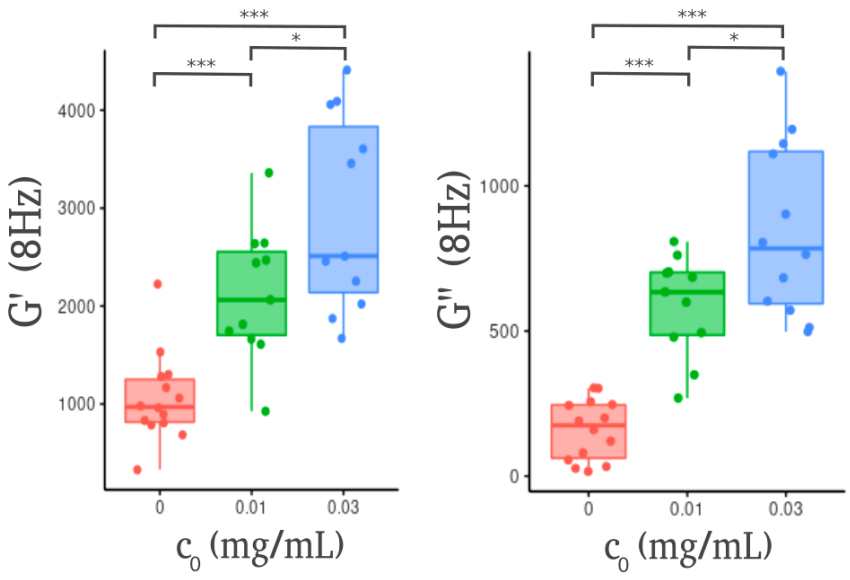

Figure 5: Statistical significance showing differences in moduli G' and G'' (in Pa) at 8 Hz. ANOVA test was carried out as explained in §2.5. * $p < 0.05$, ** $p < 0.01$, *** $p < 0.001$.

ing first (negative power law exponent a ~ -0.05), then increasing at higher frequencies like a fluid (slope c ~ 1). The values are comparable to what is usually found for single cells, typically in the range [500-2,000 Pa] (Lekka et al. (1999); Abidine et al. (2015); Yubero et al. (2020)).

- On the other hand, with the presence of collagen (c_0 = 0.01 mg/mL and c_0 = 0.03 mg/mL), the power law behavior for G' changes and exhibits a different exponent $a \sim 0.12$, corresponding to a more glassy regime (Sollich et al. (1997)). G'' exhibits a similar exponent (b ~ 0.12) at low frequencies but then increases more with a slope c=1 at higher frequencies.

- Comparing the two collagen concentrations, the exponents a seem to be the same, but there is reinforcement (larger G' and G'') for the larger concentration c_0 = 0.03 mg/mL due to the

possible presence of extra collagen fibers, with respect to the case c_0 = 0.01 mg/mL.

- The transition frequency f_T, separating the glassy behavior from the viscous regime (at high frequencies) can be found solving $G'(f_T) = G''(f_T)$ or $G_0\, f_T^a = G_1\, f_T^b + G_2\, f_T$. The solution can be found analytically for c_0 = 0.01 and 0.03 mg/mL because $a = b$ whereas in the case c_0 =0 mg/mL, a few iterations are necessary to obtain f_T. We find the respective transition frequencies (f_T) 197 Hz, 182 Hz and 170 Hz corresponding to c_0 = 0, 0.01, 0.03 mg/mL (also listed in Table 1).

- Note that the rheology of the collagen solutions prepared with culture medium has been measured separately using a classical rheometer (Anton Paar, model MCR 301, cone–plate geometry, diameter 5 cm, cone angle 0.5°, T=37°C): η_0 = 0.8 mPa.s, $\eta_{0.01}$ = 0.99 $f^{-0.044}$ mPa.s and $\eta_{0.03}$ = 9.1 $f^{-0.46}$ mPa.s (with a constant shear rate $\dot{\gamma} = 2\,\pi$ f, and 10 Hz < f < 100 Hz). This shows a Newtonian behavior for the solution without collagen, a very slight non-Newtonian effect at c=0.01 mg/mL (slope −0.044), and a more pronounced effect at c=0.03 mg/mL (slope −0.46). But these non–Newtonian effects are not sufficient to explain the drastic changes occuring with the spheroid rheology already observed at c_0=0.01 mg/mL as shown in Figure 4.

3.2. Confocal microscopy

Confocal microscopy images were acquired as described in §2.4, and images taken from Z–stacks were selected to represent the general picture of the spheroids as well as the presence of collagen, in order to test whether it has been diffusing through the spheroid. Three typical images of such spheroids are shown in Figure 6. It can be seen from these images that the collagen has

penetrated within the spheroid. Spheroids with collagen look more compact with cells fermly embedded within the matrix. On the other hand, it seems that the spheroid without collagen lacks cohesion with cells spreading slightly towards the outside. The effect can also be seen in Figure 2 with some cells spreading also for c_0 = 0 mg/mL. These effects, together with the measurements of dynamic moduli, will be discussed in the next part.

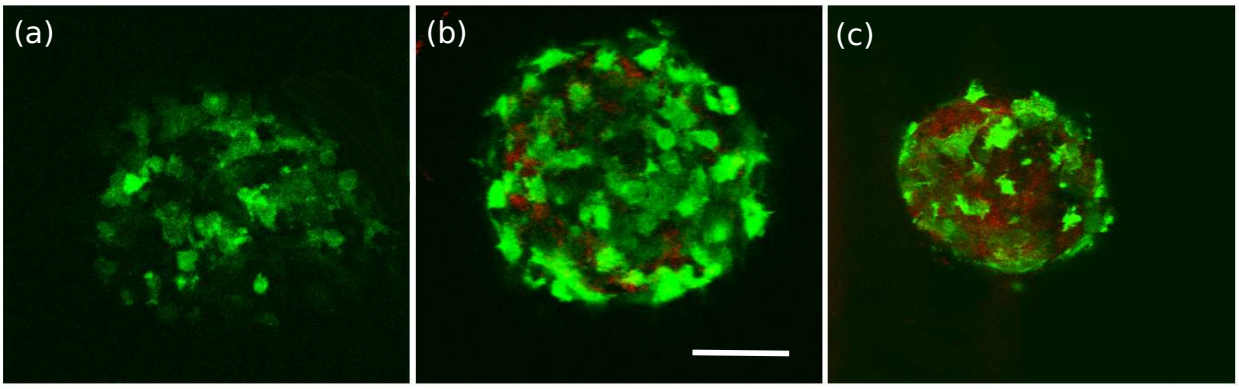

Figure 6: Confocal microstructure of spheroids without or with collagen. Actin-GFP labeled cells appear in green, wheras collagen, imaged by reflectance is shown in red. (a) c_0=0 (b) c_0=0.01mg/mL (c) c_0=0.03 mg/mL of collagen. Scale bar = 100 μm (same for the three images). Images are projections of 5 slices located at the mid–plane.

4. Discussion

Multicellular spheroids have been studied in the past, and are now considered as a good tumor model, but their mechanical properties remain insufficiently explored. Still these properties are essential to understand the tumor–stroma interactions (Provenzano et al. (2006); Kai et al. (2019); Natarajan et al. (2019)). Interesting works applying homogeneous pressures are available (Delarue et al. (2013)) while measuring local stresses (Dolega et al. (2017)). The global properties have been measured (Marmottant et al. (2009)) in compression–relaxation tests only and other elegant

techniques have been developped using Brillouin light scattering (Yan et al. (2022)). But there is a lack regarding general rheological properties in terms of deformation rate, and in function of the composition of spheroids, i.e. the ECM content. This is what we analyzed in this work using AFM microrheology.

First we used an alternative way to prepare spheroids (Figure 1) using hanging drops, thus avoiding adhesion to the substrate; this allowed us to prepare well–controlled spheroids (size and microstructure) at different collagen contents (Figure 2). Methods developped in culture wells are also available (Abidine et al. (2021)) but can still lead to cell adhesion at the bottom of wells, in the case of ECM addition. Then we used a previous AFM methodology (see Figure 3) to investigate the rheology of such spheroids (Giannetti et al. (2020); Abidine et al. (2021)) and obtained viscoelastic data covering three decades in frequency (Figure 4)). The method has already been shown to provide interesting features to compare biological tissues in healthy and modified conditions, such as chondrocytes–based tisues, cartilages or tendons (Lee et al. (2010); Nia et al. (2013); Connizzo and Grodzinsky (2017)). Our data shows that spheroids that have grown three days without collagen present a classical rheological behavior – close to cell behavior and its relevant values between 500 and 2,000 Pa (Lekka et al. (1999); Abidine et al. (2015)) – with a very slowly evolving elastic modulus G' (slope 0.05) and a viscous one (G'') first decreasing, then increasing with a slope of 1 at higher frequencies. On the other hand, as spheroid growth is held within a collagen solution (0.01 mg/mL or 0.03 mg/mL), the behavior changes drastically: a slow increase of G' is found (same slope of 0.12) vs. frequency for both cases whereas G'' has the same behavior only at small frequencies (slope 0.12), but increases faster (slope 1) at higher ones. Finally significant differences were found between the three types of spheroids (Figure 5),

thus AFM microrheology appears as a robust technique of investigation to compare them. This behavior has been found previously for individual cells (Fabry et al. (2001); Alcaraz et al. (2002); Abidine et al. (2015)) and can be described using soft rheology models (Sollich et al. (1997); Fabry et al. (2001); Alcaraz et al. (2003)).

As we wanted to build a model able to predict the three cases, we used a different approach allowing to present two different slopes for G' and G'' at smaller frequencies, i.e. $G' = G_0\, f^a$, $G'' = G_1\, f^b + G_2\, f^c$. We found that $c = 1$ for all cases (c_0=0, 0.01, 0.03 mg/mL) and $a = b = 0.12$ for cases with collagen. For c_0=0 (no collagen), it was found that $a = 0.05$ but b is negative: $b = -0.05$ (see Table 1). Finally, the investigation of the transition frequency f_T, as defined previously (Abidine et al. (2018)), showed a decrease with collagen content, thus collagen plays the role of a glassy agent, and parameter f_T can be considered as a rheology marker.

The interpretation of such data is novel, as it brings into play the intriguing role of collagen, in particular, under such conditions, collagen is merely a viscous fluid, thus it could seem unexpected to find such different properties going from elastic–like behavior to the glassy state, characterized by constant slopes for G' and G'' at low frequencies (Sollich et al. (1997)). Separate measurements showed that collagen at such small concentrations exhibits a Newtonian behavior (0 and 0.01 mg/mL) and a shear–thinning behavior at the higher concentration (0.03 mg/mL). Therefore, this is not sufficient to explain the change in spheroid rheology observed in Figure 4. As a consequence the response lies in the microstructure of such spheroids. At smaller scales, as observed in Figure 6, the collagen network contains fibers acting as a backbone to allow cells to bind. This is indeed shown in Figure 6a where cells without collagen are not bound together and the spheroid does not appear well packed. On the other hand, one can clearly see that the structure of spheroids is more

compact with the addition of collagen but the spheroid size is different (Figure 2 and Figure 6).

With the increase of collagen content (higher red intensity levels shown in Figure 6), it seems that cells spread well and exhibit more pointed protrusions (with possible adhesions) as shown in our previous work (Iordan et al. (2010)). It is known that T24 cells do not develop enough E–cadherins (Bindels et al. (2000)) and that the expansion of bladder carcinoma cells is limited, therefore the microstructure modified by cell–collagen interactions is essential to enhance the formation of such spheroids. Note that the role of ECM has already been pointed out to be a pressure sensor and a regulator of tumor spheroids (Dolega et al. (2021)). In this latter work, the ECM space (not necessarily collagen) was estimated to be 15% in volume. Here the collagen content is difficult to estimate but is shown (Figure 6) to enhance the formation of a more regular spheroid. This is possibly due to the fact that the extracellular matrix allows cancer cells to bind more efficiently during spheroid formation. Altogether this rigidifies the spheroid from a macroscopic point of view, and increases G' and G'' moduli. The resulting behavior is that of a glassy system (Sollich et al. (1997)) already observed with single cells (Trepat et al. (2008)), allowing cancer cell dynamics (Abidine et al. (2018)) to change constantly through metastable states, this being in favor of tumor invasion.

5. Conclusion

Collagen is therefore an essential component allowing cells to bind and form a homogeneous medium, in the case of spheroids. AFM microrheology was shown to be a very valuable tool allowing to capture these changes due to the presence of collagen, and a soft rheology model was found suitable to predict such behaviors. Confocal microscopy also enabled us to go deeper into

the spheroids by observing differences in microstructure; this needs to be investigated further to capture the fine interactions between cells and collagen fibers using adequate antibodies/markers. Future works should focus on the ability of various bladder cancer cells to form stable tumors depending on the amount of E–cadherins, collagen content and cell invasiveness. This would help to understand how tumors can sense/use the micro–environment to grow in size, and how collagen deposition can be correlated with the rheological properties.

Declarations

Funding: C.V. is a member of the LabeX Tec 21 (Investissements d'Avenir:grant agreement No. ANR-11-LABX-0030) and is thankful for the access to the confocal microscope facility.

Acknowledgments: The authors are thankful to G. Cappello and P. Recho (LIPhy) for valuable discussions and suggestions regarding the topic of this work.

Availability of data and material: All the relevant data are available upon request.

Declaration of Competing Interest

The authors declare that they have no known competing financial interests or personal relationships that could have appeared to influence the work reported in this paper.

References

Abidine, Y., Constantinescu, A., Laurent, V.M., Rajan, V.S., Michel, R., Laplaud, V., Duperray, A., Verdier, C., 2018. Mechanosensitivity of cancer cells in contact with soft substrates using AFM. Biophys. J. 114, 1165–1175.

Abidine, Y., Giannetti, A., Revilloud, J., Laurent, V.M., Verdier, C., 2021. Viscoelastic properties in cancer: from cells to spheroids. Cells 10, 1704.

Abidine, Y., Laurent, V.M., Michel, R., Duperray, A., Verdier, C., 2015. Local mechanical properties of bladder cancer cells measured by AFM as a signature of metastatic potential. Eur. Phys. J. Plus 130, 202.

Alcaraz, J., Buscemi, L., Grabulosa, M., Trepat, X., Fabry, B., Farré, R., Navajas, D., 2003. Microrheology of human lung epithelial cells measured by atomic force microscopy. Biophys. J. 84, 2071–2079.

Alcaraz, J., Buscemi, L., de Morales, M.P., Colchero, J., Baro, A., Navajas, D., 2002. Correction of microrheological measurements of soft samples with atomic force microscopy for the hydrodynamic drag on the cantilever. Langmuir 18, 716–721.

Bindels, E.M., Vermey, M., van den Beemd, R., Dinjens, W.N., Kwast, T.H.V.D., 2000. E-cadherin promotes intraepithelial expansion of bladder carcinoma cells in an in vitro model of carcinoma in situ. Cancer Res. 60, 177–183.

Butt, H.J., Jaschke, M., 1995. Calculation of thermal noise in atomic force microscopy. Nanotechnology 6, 1–7.

Cai, P., Mizutani, Y., Tsuchiya, M., Maloney, J.M., Fabry, B., Vliet, K.J.V., Okajima, T., 2013. Quantifying cell-to-cell variation in power-law rheology. Biophys. J. 105, 1093–1102.

Chotard-Ghodsnia, R., Haddad, O., Leyrat, A., Drochon, A., Verdier, C., Duperray, A., 2007. Morphological analysis of tumor cell/endothelial cell interactions under shear flow. J. Biomech. 40, 335–344.

Connizzo, B.K., Grodzinsky, A.J., 2017. Tendon exhibits complex poroelastic behavior at the nanoscale as revealed by high-frequency AFM-based rheology. J. Biomech. 54, 11–18.

Cross, S.E., Jin, Y.S., Rao, J., Gimzewski, J.K., 2007. Nanomechanical analysis of cells from cancer patients. Nat. Nanotechnol. 2, 780–783.

Delarue, M., Montel, F., Caen, O., Elgeti, J., Siaugue, J.M., Vignjevic, D., Prost, J., Joanny, J.F., Cappello, G., 2013. Mechanical control of cell flow in multicellular spheroids. Phys. Rev. Letters 110.

Delarue, M., Montel, F., Vignjevic, D., Prost, J., Joanny, J.F., Cappello, G., 2014. Compressive stress inhibits proliferation in tumor spheroids through a volume limitation. Biophys. J. 107, 1821–1828.

Dolega, M., Zurlo, G., Goff, M.L., Greda, M., Verdier, C., Joanny, J.F., Cappello, G., Recho, P., 2021. Mechanical behavior of multi-cellular spheroids under osmotic compression. J. Mech. Phys. Solids 147, 104205.

Dolega, M.E., Delarue, M., Ingremeau, F., Prost, J., Delon, A., Cappello, G., 2017. Cell-like pressure sensors reveal increase of mechanical stress towards the core of multicellular spheroids under compression. Nat. Comm. 8, 14056.

Fabry, B., Maksym, G.N., Butler, J.P., Glogauer, M., Navajas, D., Fredberg, J.J., 2001. Scaling the microrheology of living cells. Phys. Rev. Lett. 87, 148102.

Friedl, P., Borgmann, S., Bröcker, E.B., 2001. Amoeboid leukocyte crawling through extracellular matrix: lessons from the dictyostelium paradigm of cell movement. J. Leukoc. Biol. 70, 491–509.

Fung, Y.C., 1993. Biomechanics. Mechanical properties of living tissues. Springer-Verlag, New York.

Giannetti, A., Revilloud, J., Verdier, C., 2020. Mechanical properties of 3d tumor spheroids measured by afm. Comput. Meth. Biomech. Biomed. Eng. 23, S125–127.

Haddad, O., Chotard-Ghodsnia, R., Verdier, C., Duperray, A., 2010. Tumor cell/endothelial cell tight contact upregulates endothelial adhesion molecule expression mediated by nfkb: differential role of the shear stress. Exp. Cell Res. 316, 615–626.

Helmlinger, G., Netti, P.A., Lichtenbeld, H.C., Melder, R.J., Jain, R.K., 1997. Solid stress inhibits the growth of multicellular tumor spheroids. Nat. Biotechnol. 15, 778–783.

Iordan, A., Duperray, A., Gérard, A., Grichine, A., Verdier, C., 2010. Breakdown of cell-collagen networks through collagen remodeling. Biorheology 47, 277–295.

Iordan, A., Duperray, A., Verdier, C., 2008. Fractal approach to the rheology of concentrated cell suspensions. Phys. Rev. E 77, 011911.

Kai, F., Drain, A.P., Weaver, V.M., 2019. The extracellular matrix modulates the metastatic journey. Dev. Cell 49, 332–346.

Kuo, C.T., Wang, J.Y., Lin, Y.F., Wo, A.M., Chen, B.P.C., Lee, H., 2017. Three-dimensional spheroid culture targeting versatile tissue bioassays using a pdms-based hanging drop array. Sci. Rep. 7, 4363.

Laurent, V.M., Duperray, A., Sundar, V.R., Verdier, C., 2014. Atomic force microscopy reveals a role for endothelial cell icam-1 expression in bladder cancer cell adherence. PLOS One 9, e98034.

Lee, B., Han, L., Frank, E.H., Chubinskaya, S., Ortiz, C., Grodzinsky, A.J., 2010. Dynamic mechanical properties of the tissue-engineered matrix associated with individual chondrocytes. J. Biomech. 43, 469–476.

Lekka, M., Laidler, P., Gil, D., Lekki, J., Stachura, Z., Hrynkiewicz, A.Z., 1999. Elasticity of normal and cancerous human bladder cells studied by scanning force microscopy. Eur. Biophys. J. 28, 312–316.

Levental, I., Georges, P.C., Janmey, P.A., 2007. Soft biological materials and their impact on cell function. Soft Matter 3, 299–306.

Marmottant, P., Mgharbel, A., Käfer, J., Audren, B., Rieu, J.P., Vial, J.C., van der Sanden, B., Marée, A.F.M., Graner, F., Delanoë-Ayari, H., 2009. The role of fluctuations and stress on the effective viscosity of cell aggregates. Proc. Natl Acad. Sci. USA 106, 17271–17275.

Mierke, C.T., 2019. The matrix environmental and cell mechanical properties regulate cell migration and contribute to the invasive phenotype of cancer cells. Rep. Prog. Phys. 82, 064602.

Natarajan, S., Foreman, K.M., Soriano, M.I., Rossen, N.S., Shehade, H., Fregoso, D.R., Eggold, J.T., Krishnan, V., Dorigo, O., Krieg, A.J., Heilshorn, S.C., Sinha, S., Fuh, K.C., Rankin, E.B., 2019. Collagen remodeling in the hypoxic tumor-mesothelial niche promotes ovarian cancer metastasis. Cancer Res. 79, 2271–2284.

Netti, P.A., Roberge, S., Boucher, Y., Baxter, L.T., Jain, R.K., 1996. Effect of transvascular fluid exchange on pressure-flow relationship in tumors: a proposed mechanism for tumor blood flow heterogeneity. Microvasc. Res. 52, 27–46.

Nia, H., Bozchalooi, I., Li, Y., Han, L., Hung, H.H., Frank, E., Youcef-Toumi, K., Ortiz, C., Grodzinsky, A., 2013. High-bandwidth afm-based rheology reveals that cartilage is most sensitive to high loading rates at early stages of impairment. Biophys. J. 104, 1529–1537.

Palade, L.I., Vernay, V., Attané, P., 1996. A modified fractional model to describe the entire viscoelastic behavior of polybutadienes from flow to glassy regime. Rheol. Acta 35, 265–273.

Preziosi, L., Ambrosi, D., Verdier, C., 2010. An elasto-visco-plastic model of cell aggregates. J. Theor. Biol. 262, 35–47.

Provenzano, P.P., Eliceiri, K.W., Campbell, J.M., Inman, D.R., White, J.G., Keely, P.J., 2006. Collagen reorganization at the tumor-stromal interface facilitates local invasion. BMC Medicine 4, 38.

Quarto, G., Spinelli, L., Pifferi, A., Torricelli, A., Cubeddu, R., Abbate, F., Balestreri, N., Menna, S., Cassano, E., Taroni, P., 2014. Estimate of tissue composition in malignant and benign breast lesions by time-domain optical

mammography. Biomedical optics express 5, 3684–3698.

Rajan, V.S., Laurent, V.M., Verdier, C., Duperray, A., 2017. Unraveling the receptor-ligand interactions between bladder cancer cells and the endothelium using AFM. Biophys. J. 112, 1246–1257.

Riedl, J., Crevenna, A.H., Kessenbrock, K., Yu, J.H., Neukirchen, D., Bista, M., Bradke, F., Jenne, D., Holak, T.A., Werb, Z., Sixt, M., Wedlich-Soldner, R., 2008. Lifeact: a versatile marker to visualize F-actin. Nat. Methods 5, 605–607.

Sollich, P., Lequeux, F., Hébraud, P., Cates, M.E., 1997. Rheology of soft glassy materials. Phys. Rev. Letters 78, 2020–2023.

Stamenovic, D., Rosenblatt, N., Montoya-Zavala, M., Matthews, B.D., Hu, S., Suki, B., Wang, N., Ingber, D.E., 2007. Rheological behavior of living cells is timescale-dependent. Biophys. J. 93, L39–L41.

Trepat, X., Lenormand, G., Fredberg, J.J., 2008. Universality in cell mechanics. Soft Matter 4, 1750–1759.

Weiswald, L.B., Bellet, D., Dangles-Marie, V., 2015. Spherical cancer models in tumor biology. Neoplasia 17, 1–15.

Whatcott, C.J., Diep, C.H., Jiang, P., Watanabe, A., LoBello, J., Sima, C., Hostetter, G., Shepard, H.M., Von Hoff, D.D., Han, H., 2015. Desmoplasia in primary tumors and metastatic lesions of pancreatic cancer. Clin. Cancer Res. 21, 3561–3568.

Xu, S., Xu, H., Wang, W., Li, S., Li, H., Li, T., Zhang, W., Yu, X., Liu, L., 2019. The role of collagen in cancer: from bench to bedside. J. Transl. Med. 17, 309.

Yan, G., Monnier, S., Mouelhi, M., Dehoux, T., 2022. Probing molecular crowding in compressed tissues with brillouin light scattering. Proc. Natl Acad. Sci. USA 119, e2113614119.

Yubero, M.L., Kosaka, P.M., San Paulo, A., Malumbres, M., Calleja, M., Tamayo, J., 2020. Effects of energy metabolism on the mechanical properties of breast cancer cells. Commun. Biology 3, 590.